Available online at www.sciencedirect.com
SCIENCE DIRECT®
Biochemical and Biophysical Research Communications 338 (2005) 198–205
BBRC
www.elsevier.com/locate/ybbrc

Structure of catechol 1,2-dioxygenase from *Pseudomonas arvilla*

Cathleen A. Earhart [a], Matthew W. Vetting [a,1], Ramachandraiah Gosu [a], Isabelle Michaud-Soret [b,2], Lawrence Que Jr. [b], Douglas H. Ohlendorf [a,*]

[a] *Department of Biochemistry, Molecular Biology, and Biophysics and Center for Metals in Biocatalysis, University of Minnesota, 6-155 Jackson Hall, 321 Church St. SE, Minneapolis, MN 55455, USA*
[b] *Department of Chemistry, Center for Metals in Biocatalysis, University of Minnesota, Minneapolis, MN 55455, USA*

Received 15 July 2005
Available online 8 September 2005

Abstract

Catechol 1,2-dioxygenase was first studied by Hayaishi and colleagues in 1950. In 1967, catechol 1,2-dioxygenase from *Pseudomonas arvilla* C-1 (PaCTD) was chosen as a model system for the catecholic intradiol dioxygenases due to its activity, stability, and expression level. Here we report the 2.65 Å structure of the ββ isozyme of PaCTD. The structure supports the hypothesis first made by Vetting and Ohlendorf [The 1.8 Å crystal structure of catechol 1,2-dioxygenase reveals a novel hydrophobic helical zipper as a subunit linker, Struct. Fold. Des. 8 (2000) 429–440.] that the catechol 1,2-dioxygenases are lipid binding proteins. The 5 amino-terminal helices involved in dimerization and forming the lipid binding site are shown to be plastic in their positions and orientations. The sequence differences between the α and β polypeptides are located at the part of the monomers distant from dimerization surface and thus permit the formation of the 3 isozymes (αα, αβ, and ββ) of PaCTD. The reported inactivation by sulfhydryl-modifying reagents is explained by the structure. The 10-residue Helix F (residues 203–212) is proposed to be central in communicating between the lipid binding site and the active site.

Keywords: X-ray crystallography; Metalloenzyme; Lipid binding protein; Nonheme iron; Intradiol dioxygenase

The first biochemical study of pyrocatechase (catechol 1,2-dioxygenase; 1,2-CTD) was reported by Hayaishi and Hashimoto [1]. In 1957, Hayaishi et al. [2] succeeded in purifying 12 mg of pyrocatechase from 10 g of *Pseudomonas fluorescens*. After screening 20 strains of various soil bacteria, Dr. Hayaishi's laboratory focused on *Pseudomonas arvilla* C-1 where they were able to obtain pyrocatechase with 50% higher specific activity than that from *P. fluorescens* [3]. It is this pyrocatechase from *P. arvilla* C-1 (PaCTD) that has become the model 1,2-CTD for kinetic and spectroscopic studies.

1,2-CTD, protocatechuate 3,4-dioxygenase (3,4-PCD), and hydroxyquinol 1,2-dioxygenase (1,2-HQD) catalyze the intradiol cleavage by molecular oxygen of their respective catecholic substrates using only a nonheme ferric ion as a cofactor. Structural studies [4–6] have corroborated the models proposed by Whittaker and Lipscomb [7] and Pyrz et al. [8] in which the iron is ligated by two histidines and two tyrosines. The initial coordination geometry is trigonal bipyramidal with one tyrosine, one, histidine and a bound hydroxyl in the equatorial plane, and the other tyrosine and histidine as axial ligands [4–6]. Structures of complexes of 3,4-PCD and 1,2-CTD from *Acinetobacter* strain ADP1 (AcCTD) with substrates and inhibitors show the axial tyrosine dissociates upon iron chelation by substrate [4,6,9,10].

AcCTD, chlorocatechol 1,2-dioxygenase (1,2-ClCTD) from *Rhodococcus opacus* 1CP and 1,2-HQD from *Nocardioides simplex* 3E (the catecholic 1,2-dioxygenases from

* Corresponding author. Fax: +1 612 624 5121.
E-mail address: ohlen@umn.edu (D.H. Ohlendorf).
[1] Present address: Department of Biochemistry, Albert Einstein College of Medicine, 1300 Morris Park Avenue, Bronx NY 10461-1602, USA.
[2] Present address: Laboratoire de Physicochimie des Métaux en Biologie, UMR CNRS-CEA-UJF 5155, DRDC/CEA-Grenoble, 17 Avenue des Martyrs, 38054 Grenoble Cedex 9, France.

0006-291X/$ - see front matter © 2005 Elsevier Inc. All rights reserved.
doi:10.1016/j.bbrc.2005.08.221

which structures have been determined) are homodimers of a single polypeptide. In contrast, PaCTD exists as 3 isozymes, αα, αβ, and ββ, formed by 2 polypeptides, α and β, with molecular masses of 29.5 and 33.4 kDa, respectively [11,12]. Here we report the structure of the ββ isozyme of 1,2-CTD from *P. arvilla* C-1 and discuss emerging generalizations regarding the 1,2-CTDs and other catecholic 1,2-dioxygenases.

Materials and methods

Protein purification and crystallization. PaCTD was purified from *P. arvilla* C-1 (ATCC 23974) and crystallized using hanging drop techniques as described in Earhart et al. [13].

Data collection. Diffraction data were collected in-house at room temperature using a Bruker-Siemens High Star area detector mounted on a Rigaku RU200 rotating anode generator producing monochromatized Cu–Kα radiation. These data were scaled and merged using the program XENGEN [14]. Data collection and processing statistics are summarized in Table 1.

Structure solution and refinement. The structure PaCTD was solved by molecular replacement using XPLOR [15] and the structure of AcCTD (PDB entry = 1DLM) as a probe. Refinement of the structural model was performed using XPLOR and CNS [16] with 5% of the data set aside from the start of refinement to assess the progress of refinement using the free *R* value [17]. Structural models were visually examined using O [18]. Model quality was monitored using PROCHECK [19].

Results and discussion

Fold of PaCTD monomer

The ββ isozyme of PaCTD crystallizes with one monomer in the crystallographic asymmetric unit. Of the 310 residues in this polypeptide, all residues have very good density, except for the amino terminal threonine and residues 268–277. The structure is very similar to that of AcCTD which is 53% identical in sequence. PaCTD begins with five α-helices (Fig. 1). Helices B, C, and D of the two monomers form a hydrophobic cavity at the dimeric interface that contains two lipid molecules (Fig. 2). The lipids are modeled as phosphatidylcholine although electron density is inadequate to identify the head group. The fatty acid chains were built as palmitic and capric acids to agree with the electron density. The discovery that the dimeric catechol intradiol dioxygenases are lipid-binding proteins was reported in 2000 [4]. Mass spectrometry of that 1,2-CTD displayed peaks with masses consistent with lipids [4]. The structure described here plus those of 1,2-ClCTD from *Rhodococcus opacus* 1CP [20] and 1,2-HQD from *Nocardioides simplex* 3E [6] supports this general lipid-binding property.

The fold of the lipid-binding domain is unique. Fatty acid binding proteins [21] and lipocalins [22] are composed almost entirely of β strands. The START domain of phosphatidylcholine transfer protein has an α/β-fold and binds a nearly completely buried lipid at the α–β interface [23]. Only nonspecific lipid transfer protein (NS-LTP) from wheat [24] and that from saposin B [25] are α-helical proteins. NS-LTP has a 4 α-helical bundle with 2 lipids binding in its hydrophobic center [24]. In saposin, B the lipid is bound between two hairpins each formed by four α-helices [25]. Superposition of the lipid-binding domain of PaCTD

Table 1
Data processing and refinement

Data processing	
Space group	$C222_1$
Unit cell axes (Å)	$a = 62.7$, $b = 71.5$, $c = 187.1$
Resolution (Å)	2.6
Unique reflections	11,001
Completeness (%)	91
$\langle I/\sigma \rangle$	10.0
R_{sym}	0.079
Molecules in asymmetric unit	1
Refinement	
Protein atoms	2411
Lipid atoms	44
Iron atoms	1
R factor	0.229
Free *R*	0.284
RMS deviation from ideality	
Bond lengths (Å)	0.013
Bond angles (°)	2.0
Ramachandran plot (%)	
Most-favored region	86.6
Additionally allowed	9.9
Generously allowed	2.7

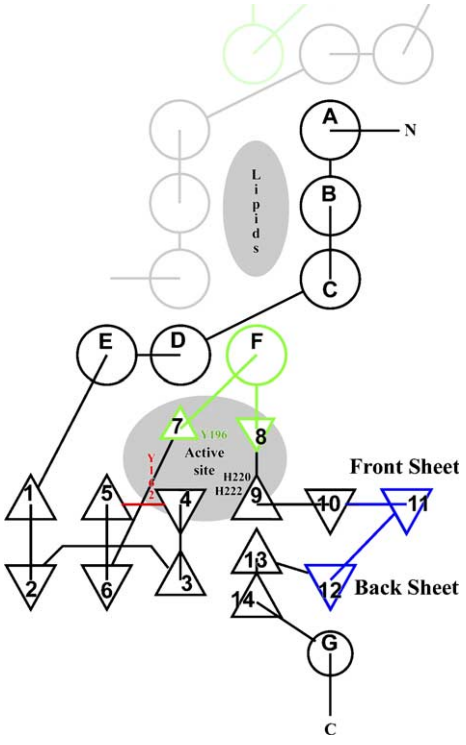

Fig. 1. Topology drawing of PaCTD dimer. Triangles indicate β strands. Circles indicate helices. Finger 1 is red, Finger 2 is green, and Finger 3 is blue. The second monomer in the dimer is drawn with lighter lines. The site for binding lipids and the active site are indicated as are the Fe ligands.

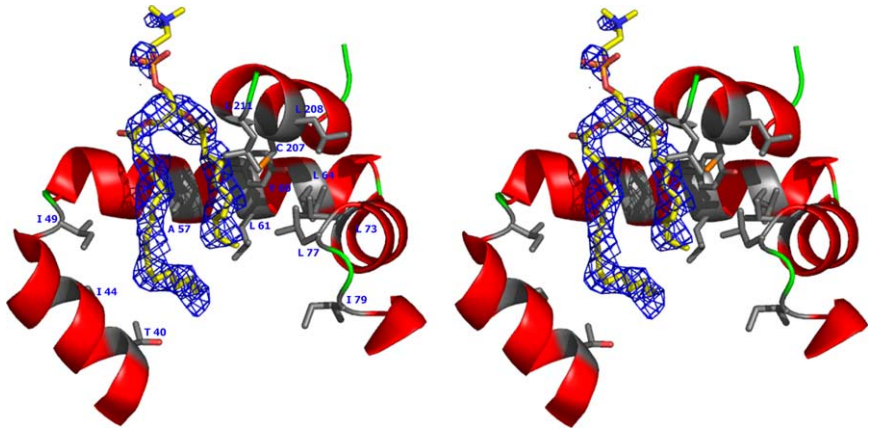

Fig. 2. Stereo drawing of lipid-binding site of PaCTD. Residues within van der Waals distance of the lipid and contained in this section are shown as sticks and are labeled. The $2F_o - F_c$ electron density for the lipid is contoured at 1σ.

and those of NS-LTP and saposin B show no significant structural homology.

The physiological function for the bound lipid is unknown. A recent study by Citadini et al. [26] studied the binding of various lipids to 1,2-ClCTD from *Pseudomonas putida*. Their measurements using spin-labeled lipids are consistent with lipids binding with their hydrophobic tails buried and their hydrophilic head groups exposed precisely as the structural data suggest. Their studies with stearic acid led them to suggest that lipid binding inhibits dioxygenase activity. But the protein we purified in this study and those purified by us and others in [4,6,20] have lipid bound, as the structures indicate, yet have normal, activity. In fact, we were unable to remove the lipid even using a Lipidex column. Thus, the inhibition observed by Citadini et al. [26] with the addition of stearic acid may be the result of displacing another lipid.

Helix D ends with the Gly 76-Leu 77-Gly 78 sequence which introduces a 114° kink to start Helix E. This GLG sequence is conserved in nearly all the 1,2-HQDs and the 1,2-CTDs (Fig. 3). The 1,2-ClCTDs typically have two fewer residues in this kink and put a large hydrophobic (phenylalanine or tryptophan) in the space occupied by Leu 77 [20]. The end of Helix D and the start of Helix E are important as they form part of the boundary between the lipid-binding site and the active site adjacent to the C3 and C4 positions of substrate (Fig. 4). As such this region is a prime candidate for communication between the lipid-binding site and the active site. One can speculate that Helix E may allow the bound lipid to modulate substrate selectivity.

The rest of the PaCTD monomer is composed primarily of β strands and has the same basic fold seen in all other intradiol dioxygenases. The fold has been compared to a hand with three fingers curling over the palm [27]. The β strands are arranged into two sheets, one of which forms the palm (front sheet in Fig. 1) and the other forms the back of the hand (back sheet in Fig. 1). Finger 3 is formed by the loop between strands β4 and β5 (red in Fig. 1).

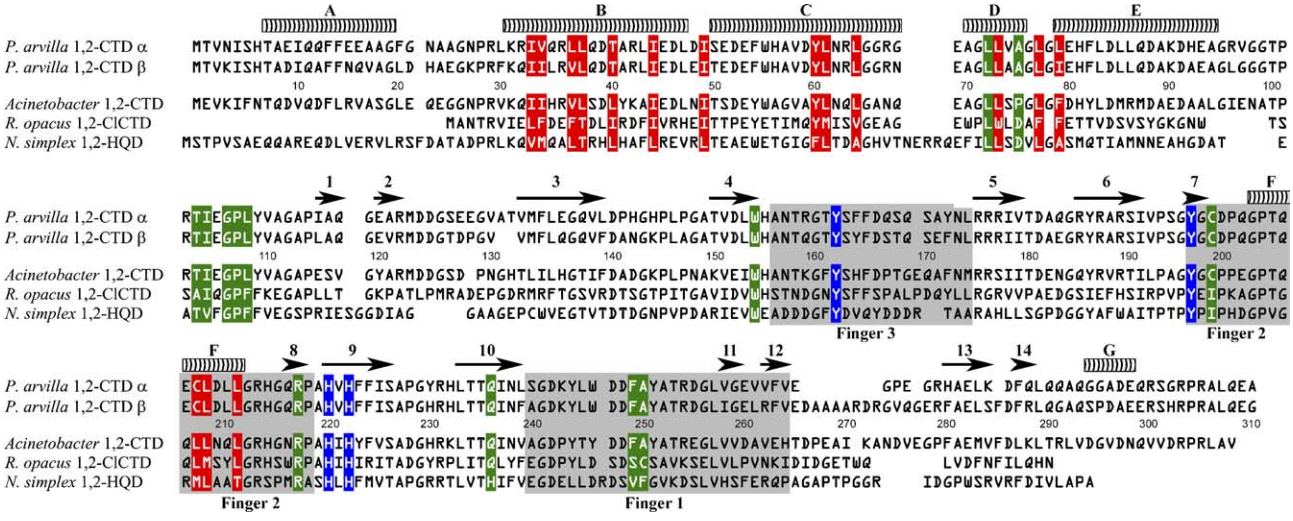

Fig. 3. Sequence alignment of selected 1,2-CTDs, ClCTDs, and 1,2-HQDs. Helices are labeled with letters and β strands with numbers. Residues highlighted in red form the lipid-binding site. Residues highlighted in blue are the Fe ligands. Residues highlighted in green form the active sites. Shaded residues make up the 3 fingers discussed in text.

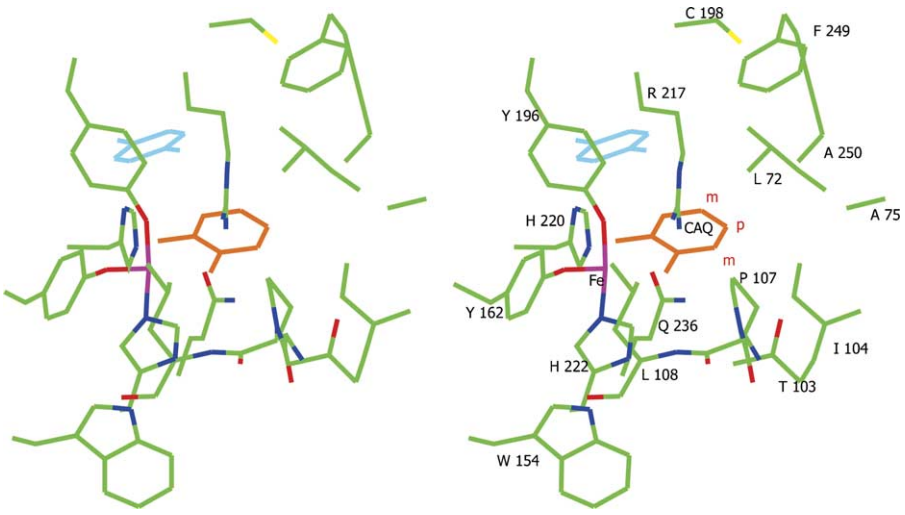

Fig. 4. Active site of PaCTD with substrate (yellow) and alternate conformation of Tyr 196 (cyan) modeled from the anaerobic complex of catechol with AcCTD [4]. The substrate substituent positions *para* (p) and *meta* (m) to the substituent hydroxyl displacing Tyr 196 are indicated.

Finger 2 is the segment between strands β6 and β9, and contains the short β7–β8 duplex and Helix F (green in Fig. 1). Finger 1 is the segment between strands β10 and β13/β14 containing strands β11 and β12. The loops at the wrist (end of β sheets away from the fingers) are small with little variations.

Superposition of the 100 core Cα's of this fold produces an RMS difference of 0.64 Å against AcCTD, 0.87 Å against 1,2-HQD, and 0.99 Å against 1,2-ClCTD, indicating that the fold is highly conserved. For the β-chain of 3,4-PCD the RMS difference with PaCTD is just slightly higher, e.g., 1.21 Å. The edge of the two β sheets farthest from the active site is one place where 1,2-CTD, 1,2-HQD, and 1,2-ClCTD differ, as a group, from 3,4-PCD. Here are strands β1 and β2 which are not present in 3,4-PCD. The second consistent variation is Finger 1 where in 3,4-PCD there are three short helices followed by a short β strand and a 3_{10} helix. In 1,2-CTD, 1,2-HQD, and 1,2-ClCTD, this loop tucks under strand β8 and contributes to the active site. Finger 2 in 1,2-CTD, 1,2-HQD, and 1,2-ClCTD all have a 10 residue helix (Helix E) at the end of the loop. The first residue in Finger 2 is Tyr 196, the dissociating axial tyrosinyl Fe ligand, and in the strand immediately following Finger 2 are the two histidinyl Fe ligands. As discussed above one side of Helix F forms a substantial part of the lipid-binding site suggesting a route of communication between the active site and lipid-binding site. In 3,4-PCD, Finger 2 is just a β-duplex. However, it interacts with another 3,4-PCD β chain through a local 2-fold interaction. Thus, aggregation geometry in 3,4-PCD can be sensed by Finger 2 and this information communicated to its active site. Finger 3 is the most variable in conformation. 1,2-CTD, 1,2-HQD, and 1,2-ClCTD all have a similar number of residues and are forced away from the front sheet (palm) by the fat end of Finger 2 because of Helix F. In these proteins, residues in this loop come close to the C-terminal end of Helix C. For the 1,2-HQDs the 5-residue insertion after Helix C is responsible for some favorable charge pair and hydrogen bond interactions with both Fingers 2 and 3. Finger 3 is also notable because it contains the equatorial tyrosinyl Fe ligand, Tyr 164.

The α and β polypeptides of PaCTD are 77% identical (see Fig. 2) [28]. An analysis of the sequence differences shows that the changes are largely conservative and are spatially clustered. The fragment from residues 15 to 35, where only 41% of the residues are identical, makes up the end of Helix A and the beginning of Helix B. Nearly all these differences are at solvent exposed residues. Notably, the side chain amino group of Lys 27 in the β polypeptide (Asn in the α polypeptide) is only 2.4 Å from the lipid phosphate. This favorable electrostatic interaction promotes the binding of phospholipids. The steady state kinetic analysis [12] of the 3 PaCTD isozymes indicates identical K_m's for substrate and O_2 but some small differences in k_{cat} (54, 49, and 45 s^{-1} for the ββ, αβ, and αα isozymes, respectively). Since the rate-determining step is product release [29], it is tempting to speculate that the sequence differences between residues 15 and 25 alter vibration modes in the protein to promote substrate release.

There are one deletion and 2 insertions in the β polypeptide relative to the α. The two-residue deletion between Val 130 and Val 131 is in the loop between strands β2 and β3. The 8-residue insertion from Asp 266 to Arg 273 and the single residue insertion of Glu 278 are in the adjacent loop between strands β12 and β13/β14. As mentioned above the electron density for most of the large insertion is very poor. This region is approximately 30 Å from the nonheme iron and further from the N-terminal dimerization helices. Thus, one expects these changes not to affect the ability of PaCTD to dimerize into the αα, αβ, and ββ isozymes.

Dimerization

PaCTD like AcCTD, 1,2-ClCTD and 1,2-HQD dimerizes using a set of interlocking amino terminal helices. The overall shape of the dimer is like the letter w. The width of the dimer varies between 65 Å at the bottom of the w and 95 Å at the top. The height of the dimer ranges between 35 Å at the center to 50 Å at the ends. The thickness of the dimer is about 40 Å. The region of sequence diversity from residues 15 to 25 is at the base of the w near the 2-fold axis. The region of the insertions and deletion is at the extreme tips of the w. The active site is in the cleft between the outer wedges of the w.

At the center of the dimer is the lipid-binding site extending the thickness of the w. The residues lining the lipid-binding site are shown in Figs. 2 and 3. Ile 34 and Val 36 in β PaCTD are changed to Val 34 and Leu 36 in α PaCTD. The shift of a methylene group between these residues would have no significant structural effect since they are part of the same hydrophobic surface on the back of Helix A. Tyr 60 OH makes a hydrogen bond with the main chain O of Pro 203 helping to latch Helix F in place. This residue is either a tyrosine or tryptophan in nearly all catecholic 1,2-dioxygenases; it is a phenylalanine in the 1,2-HQDs. Ile 79 is near the end of the fatty acid chain of the bound lipid. Changing between Ile (β) to Leu (α) would place more mass closer to the fatty acid and might have a small effect on lipid binding. Both polypeptides of PaCTD have Cys 207 on Helix F in Finger 2. Cys is infrequently found in this position. Since the sulfhydryl is less than 5 Å from the lipid, modification of this residue should have a strong effect on lipid binding.

If the conserved β-fold of one monomer is used to superimpose the dimers, a significant variability in the relative orientation of the second monomer is apparent for 1,2-CTD, 1,2-ClCTD, and 1,2-HQD (Fig. 5). This variability results from small shifts in the relative orientation of the α-helices. Moving from the conserved β-fold through the five α-helices, significant changes in the helical orientations become apparent. For PaCTD and AcCTD these rotational shifts range between 1.5° and 8° (between Helices D and E). These small changes keep the overall RMS difference between the five helices of these two 1,2-CTDs to 0.73 Å. In comparing 1,2-ClCTD with PaCTD, the differences in the interhelical angles are larger and range between 7° and 11°. There is no helix A in 1,2-ClCTD. In comparing 1,2-HQD with PaCTD, the differences in the interhelical angles are even larger ranging between 12° and 42°. One of the reasons for these larger differences is the five residue insert between Helices B and C found in the 1,2-HQDs. The mobility of these helices in the catecholic 1,2-dioxygenases is a consequence of the limited hydrogen bonds between helices allowing them to easily move in response to sequence changes.

There are two other manifestations of the movements of the amino terminal helices. One is a rotation of the local

Fig. 5. Ribbon drawing of the superposition of dimers of AcCTD (green), 1,2-ClCTD (blue), and 1,2-HQD (red) onto a dimer of PaCTD (yellow) using the core conserved β fold of one monomer. The yellow sphere indicates the nonheme iron. The ball-and-stick molecules at the center of the dimers are the respective lipid molecules.

2-fold axis in the plane perpendicular to the long axis of the dimer. This rotation is 15° for 1,2-ClCTD and 19° for 1,2-HQD. A second is the rotational shift of the lipid relative to the core β fold and active site. The bound lipid is approximately 20 Å from the nonheme Fe. These distortions translate the lipid tangentially 2 Å in 1,2-ClCTD and 4 Å in HQD. This shift may alter the ability of the active site to sense the presence of lipid in the lipid-binding site.

PaCTD active site

As in other intradiol dioxygenases, the nonheme Fe is ligated by two tyrosines (Tyr 162 in Finger 3 and Tyr 196 in Finger 2) and two histidines (His 220 and His 222 in strand β9). These residues are highlighted by blue in Fig. 3; other residues lining the active site are highlighted in green. The resolution of the PaCTD structure does not allow placing of solvent molecules. However, the shape of the electron density around the nonheme Fe suggests a trigonal bipyramidal geometry identical to those of all other intradiol dioxygenases.

Work on 3,4-PCD [9,10,30,31] and AcCTD [4] shows that substrate first binds the Fe *trans* to Tyr 196 and then trans to His 222, i.e., in place of Tyr 162. In 3,

4-PCD the dissociated tyrosine is stabilized through a hydrogen bond with a tyrosine from the α chain [10]. In PaCTD there is no structurally equivalent tyrosine and thus no stabilizing hydrogen bond. Rather Leu72 which is absolutely conserved in all known dimeric catecholic 1,2-dioxygenases is at this position. Since substrate release is rate determining, eliminating an interaction that stabilizes the dissociated tyrosinyl ligand might increase k_{cat} for these enzymes.

A developing negative charge on the carbon attached to the hydroxyl that displaces Tyr 196 is then stabilized by the Arg 221-Gln 240 pair. This pair is conserved in all known 3,4-PCDs, 1,2-CTDs, and 1,2-ClCTDs while in the 1,2-HQDs the glutamine is replaced by a histidine. The shorter histidine residue at this position results in a more extended arginine side chain [6], moving the guanidinium further from the carbons of the aromatic ring towards the substituent hydroxyl relative to that seen in AcCTD [4]. Since there is no structure of a complex between a 1,2-HQD and an authentic substrate, the significance of this change remains to be analyzed.

Hayaishi's laboratory noted that activity of PaCTD could be inhibited through the action of sulfhydryl reagents such as *p*-chloromercuribenzoate, mersalyl, and mercuric chloride [2,32]. Cys 198, located on Finger 2, is the sulfhydryl that gets modified [4]. This residue forms part of the pocket into which Tyr 196 rotates upon binding substrate (see Fig. 4). Kojima et al. [3] also report that prolonged incubation in cysteine also leads to inactivation. We hypothesize that aerobic incubation in cysteine may lead to the formation of cystine disulfide bonds which would block dissociation of Tyr 196 and thus block substrate chelation.

Fujiwara et al. [32] reported that PaCTD is nearly as active toward 4-methylcatechol as catechol. Later measurements by Ridder et al. [33] indicate a reduction in k_{cat} of only 38%. 4-Methyl catechol can chelate the nonheme iron in two possible orientations. In one the methyl group is *para* to the hydroxyl that replaces Tyr 196 (*para* orientation); in the other the methyl group is *meta* to that hydroxyl (*meta* orientation). In the *meta* orientation, the methyl group would require movement of the absolutely conserved Leu 72 side chain. However in the *para* orientation, the methyl group would fit into a pocket formed by Leu 72, Ala 75, Gly 106, and Phe 107. If the methyl group is changed to a chlorine, which has a similar size but is substantially more electronegative, the observed turnover rate drops to between 2% and 6% of that observed for catechol [32,33]. A more extensive analysis by Ridder et al. [33] using a number of C4-substituted substrates revealed a strong correlation between substituent electronegativity and k_{cat}. A similar result was reported by Dorn and Knackmuss [34] in studying 1,2-ClCTD from *Pseudomonas* B13. The computational analysis by Ridder et al. relies upon a model derived from the structure of 3,4-PCD [5,27]. This model only contained the nonheme iron, its protein ligands, and the substrates under investigation. While the ligation geometries of PaCTD and 3,4-PCD are very similar, the model does not include the Arg 221-Gln 240 pair important in catalysis [35] plus the steric effects of nearby atoms. The importance of these steric effects in 1,2-CTD was earlier acknowledged by Dorn and Knackmuss [34]. In addition, Ridder et al. [33] found that electronegativity correlates only with the rates for steps involved in ring opening. Analysis of other intradiol dioxygenases indicates that product release is the rate-limiting step [29,36,37]. Thus, the reason for a correlation between substituent electronegativity and k_{cat} remains unclear.

Studies using 3-methylcatechol report reductions in turnover of about 20-fold relative to catechol [32,33]. Fe chelation with the methyl group *meta* to the hydroxyl that replaces Tyr 196 is sterically favored. The methyl group should fit into a pocket formed by Ala 75, Ile 104, and Gly 106. Gly 106 is absolutely conserved in all known catecholic intradiol dioxygenases. Ile 104 is conserved in nearly all the 1,2-CTDs and 1,2-ClCTDs. The corresponding residue in the 1,2-HQDs is valine. Ala 75 is conserved in nearly all the 1,2-CTDs. However, all the 1,2-ClCTDs and 1,2-HQDs have an aspartic acid in this position. Ala 75 is part of the kink between Helices D and E. In 1,2-CTD and 1,2-HQD this altered kink twists and translates Helix D 20° and 1.7 Å creating a space for the 3-methyl group.

Certainly we have come a long way in our understanding of the catecholic intradiol dioxygenases in the 55 years since Dr. Hayaishi started his studies of these enzymes. Nevertheless, there are still many questions remaining. For example, what is the role of the bound lipid? Will changing Gln 236 to histidine in a 1,2-CTD make it a 1,2-HQD? Are there other Fe chelation geometries, i.e., equatorial–equatorial, and do they play a role in the catalytic mechanism? Why does the rate of product release appear to depend upon substituent electronegativity? Do the sequence changes in residues 15–25 influence product release? Does having a hydrogen bond to stabilize the dissociated tyrosinyl ligand decrease product release? Future studies combining structural, mutagenic, transient kinetic, and computational analyses may provide some long awaited answers to these questions.

Note added in proof

The coordinates have been deposited in the Protein Data Bank with entry code 2AZQ.

Acknowledgments

This work has been partially supported by grants from the National Institutes of Health (GM-46436 to D.H.O., GM-33162 to L.Q.). The authors would also like to thank Ms. Debi Leverich for technical assistance, Dr. John Lipscomb for helpful discussions, the Minnesota Supercomputer

Institute for the use of computational facilities, and Mr. Ed Hoeffner for maintaining the diffraction facilities at the University of Minnesota.

Appendix A. Supplementary data

Supplementary data associated with this article can be found, in the online version, at doi:10.1016/j.bbrc.2005.08.221.

References

[1] O. Hayaishi, K. Hashimoto, Pyrocatechase. A new enzyme catalyzing oxidative breakdown of pyrocatechin, J. Biochem. (Tokyo) 37 (1950) 371–374.
[2] O. Hayaishi, M. Katagiri, S. Rothberg, Studies on oxygenases. Pyrocatechase, J. Biol. Chem. 229 (1957) 905–920.
[3] Y. Kojima, H. Fujisawa, A. Nakazawa, T. Nakazawa, F. Kanetsuna, H. Taniuchi, M. Nozaki, O. Hayaishi, Studies on pyrocatechase. I. Purification and spectral properties, J. Biol. Chem. 242 (1967) 3270–3278.
[4] M.W. Vetting, D.H. Ohlendorf, The 1.8 Å crystal structure of catechol 1,2-dioxygenase reveals a novel hydrophobic helical zipper as a subunit linker, Struct. Fold. Des. 8 (2000) 429–440.
[5] D.H. Ohlendorf, J.D. Lipscomb, P.C. Weber, Structure and assembly of protocatechuate 3,4-dioxygenase, Nature 336 (1988) 403–405.
[6] M. Ferraroni, J. Seifert, V.M. Travkin, M. Thiel, S. Kaschabek, A. Scozzafava, L. Golovleva, M. Schlomann, F. Briganti, Crystal structure of the hydroxyquinol 1,2-dioxygenase from *Nocardioides simplex* 3E, a key enzyme involved in polychlorinated aromatics biodegradation, J. Biol. Chem. 280 (2005) 21144–21154.
[7] J.W. Whittaker, J.D. Lipscomb, T.A. Kent, E. Münck, *Brevibacterium fuscum* protocatechuate 3,4-dioxygenase. Purification, crystallization, and characterization, J. Biol. Chem. 259 (1984) 4466–4475.
[8] J.W. Pyrz, A.L. Roe, L.J. Stern, L.J. Que, Model studies of iron-tyrosinate proteins, J. Am. Chem. Soc. 107 (1985) 614–620.
[9] A.M. Orville, N. Elango, J.D. Lipscomb, D.H. Ohlendorf, Structures of competitive inhibitor complexes of protocatechuate 3,4-dioxygenase—multiple exogenous ligand binding orientations within the active site, Biochemistry 36 (1997) 10039–10051.
[10] A.M. Orville, J.D. Lipscomb, D.H. Ohlendorf, Crystal structures of substrate and substrate analog complexes of protocatechuate 3,4-dioxygenase—endogenous Fe^{3+} ligand displacement in response to substrate binding, Biochemistry 36 (1997) 10052–10066.
[11] C. Nakai, H. Kagamiyama, Y. Saeki, M. Nozaki, Nonidentical subunits of pyrocatechase from *Pseudomonas arvilla* C-1, Arch. Biochem. Biophys. 195 (1979) 12–22.
[12] C. Nakai, K. Horiike, S. Kuramitsu, H. Kagamiyama, M. Nozaki, Three isozymes of catechol 1,2-dioxygenase (pyrocatechase), αα, αβ, and ββ, from *Pseudomonas arvilla* C-1, J. Biol. Chem. 265 (1990) 660–665.
[13] C.A. Earhart, M.D. Hall, I. Michaud-Soret, L. Que Jr., D.H. Ohlendorf, Crystallization of catechol-1,2 dioxygenase from *Pseudomonas arvilla* C-1, J. Mol. Biol. 236 (1994) 377–378.
[14] A.J. Howard, G.L. Gilliland, B.C. Finzel, T.L. Poulos, D.H. Ohlendorf, F.R. Salemme, Use of an imaging proportional counter in macromolecular crystallography, J. Appl. Crystallogr. 20 (1987) 383–387.
[15] A.T. Brünger, X-PLOR Version 3.1 Manual, ed., Yale University, New Haven, CT 1993.
[16] A.T. Brünger, P.D. Adams, G.M. Clore, W.L. DeLano, P. Gros, R.W. Grosse-Kunstleve, J.S. Jiang, J. Kuszewski, M. Nilges, N.S. Pannu, R.J. Read, L.M. Rice, T. Simonson, G.L. Warren, Crystallography & NMR system: a new software suite for macromolecular structure determination, Acta Crystallogr. D 54 (1998) 905–921.
[17] A.T. Brünger, Free R value: a novel statistical quantity for assessing the accuracy of crystal structures, Acta Crystallogr. D 49 (1992) 24–46.
[18] T.A. Jones, A graphics model building program and refinement system for macromolecules, J. Appl. Crystallogr. 11 (1978) 268–272.
[19] R.A. Laskowski, M.W. MacArthur, D.S. Moss, J.M. Thornton, PROCHECK: a program to check the stereochemical quality of protein structures, J. Appl. Crystallogr. 26 (1993) 283–291.
[20] M. Ferraroni, I.P. Solyanikova, M.P. Kolomytseva, A. Scozzafava, L. Golovleva, F. Briganti, Crystal structure of 4-chlorocatechol 1,2-dioxygenase from the chlorophenol-utilizing gram-positive *Rhodococcus opacus* 1CP, J. Biol. Chem. 279 (2004) 27646–27655.
[21] J.C. Sacchettini, J.I. Gordon, L.J. Banaszak, Crystal structure of rat intestinal fatty-acid-binding protein. Refinement and analysis of the *Escherichia coli*-derived protein with bound palmitate, J. Mol. Biol. 208 (1989) 327–339.
[22] D.R. Flower, A.C. North, C.E. Sansom, The lipocalin protein family: structural and sequence overview, Biochim. Biophys. Acta 1482 (2000) 9–24.
[23] S.L. Roderick, W.W. Chan, D.S. Agate, L.R. Olsen, M.W. Vetting, K.R. Rajashankar, D.E. Cohen, Structure of human phosphatidylcholine transfer protein in complex with its ligand, Nat. Struct. Biol. 9 (2002) 507–511.
[24] D. Charvolin, J.P. Douliez, D. Marion, C. Cohen-Addad, E. Pebay-Peyroula, The crystal structure of a wheat nonspecific lipid transfer protein (ns-LTP1) complexed with two molecules of phospholipid at 2.1 A resolution, Eur. J. Biochem. 264 (1999) 562–568.
[25] V.E. Ahn, K.F. Faull, J.P. Whitelegge, A.L. Fluharty, G.G. Prive, Crystal structure of saposin B reveals a dimeric shell for lipid binding, Proc. Natl. Acad. Sci. USA 100 (2003) 38–43.
[26] A. Citadini, A. Pinto, A. Araujo, O. Nascimento, A. Costa-Filho, EPR studies of chlorocatechol 1,2-dioxygenase: evidences of iron reduction during catalysis and of the binding of amphipatic molecules, Biophys. J. 88 (2005) 3502–3508.
[27] D.H. Ohlendorf, A.M. Orville, J.D. Lipscomb, Structure of protocatechuate 3,4-dioxygenase from *Pseudomonas aeruginosa* at 2.15 Å resolution, J. Mol. Biol. 244 (1994) 586–608.
[28] C. Nakai, G. Yamazaki, H. Kagamiyama, M. Nozaki, Amino acid sequence of catechol 1,2-dioxygenase (pyrocatechase) isozyme αα from *Pseudomonas arvilla* C-1, Biochem. Mol. Biol. Int. 39 (1996) 781–788.
[29] R. Viswanathan, M. Palaniandavar, T. Balasubramanian, T.P. Muthiah, Functional models for catechol 1,2-dioxygenase—synthesis, structure, spectra, and catalytic activity of certain tripodal iron(III) complexes, Inorg. Chem. 37 (1998) 2943–2951.
[30] T.E. Elgren, A.M. Orville, K.A. Kelly, J.D. Lipscomb, D.H. Ohlendorf, L. Que Jr., Crystal structure and resonance Raman studies of protocatechuate 3,4-dioxygenase complexed with 3,4-dihydroxyphenylacetate, Biochemistry 36 (1997) 11504–11513.
[31] M.W. Vetting, D.A. D'Argenio, L.N. Ornston, D.H. Ohlendorf, Structure of *Acinetobacter calcoaceticus* protocatechuate 3,4-dioxygenase at 2.2 Å resolution: Implications for the mechanism of an intradiol dioxygenase, Biochemistry 39 (2000) 7943–7955.
[32] M. Fujiwara, L.A. Golovleva, Y. Saeki, M. Nozaki, O. Hayaishi, Extradiol cleavage of 3-substituted catechols by an intradiol dioxygenase, pyrocatechase, from a Pseudomonad, J. Biol. Chem. 250 (1975) 4848–4855.
[33] L. Ridder, F. Briganti, M.G. Boersma, S. Boeren, E.H. Vis, A. Scozzafava, C. Veeger, I.M. Rietjens, Quantitative structure/activity relationship for the rate of conversion of C4-substituted catechols by catechol-1,2-dioxygenase from *Pseudomonas putida* (*arvilla*) C1, Eur. J. Biochem. 257 (1998) 92–100.

[34] E. Dorn, H.J. Knackmuss, Chemical structure and biodegradability of halogenated aromatic compounds. Substituent effects on 1,2-dioxygenation of catechol, Biochem. J. 174 (1978) 85–94.

[35] D.A. D'Argenio, M.W. Vetting, D.H. Ohlendorf, L.N. Ornston, Substitution, insertion, deletion, suppression, and altered substrate specificity in functional protocatechuate 3,4-dioxygenases, J. Bacteriol. 181 (1999) 6478–6487.

[36] H. Fujisawa, K. Hiromi, M. Uyeda, S. Okuno, M. Nozaki, Protocatechuate 3,4-dioxygenase. III. An oxygenated form of enzyme as reaction intermediate, J. Biol. Chem. 247 (1972) 4422–4428.

[37] R.W. Frazee, A.M. Orville, K.B. Dolbeare, H. Yu, D.H. Ohlendorf, J.D. Lipscomb, The axial tyrosinate Fe^{3+} ligand in protocatechuate 3,4-dioxygenase influences substrate binding and product release: evidence for new reaction cycle intermediates, Biochemistry 37 (1998) 2131–2144.